Design of a 1550 nm SiGe/Si Quantum-Well Optical Modulator

Tania Tasmin[a], Nicolas Rouger[c], Guangrui Xia[b], Lukas Chrostowski[a], and Nicolas A. F. Jaeger[a]

[a]Department of Electrical and Computer Engineering,
University of British Columbia, Vancouver, British Columbia, Canada;
[b]Department of Materials Engineering,
University of British Columbia, Vancouver, British Columbia, Canada;
[c]Grenoble Electrical Engineering Lab,
National Center for Scientific Research/ Grenoble University, France

ABSTRACT

An electrooptic modulator containing a single SiGe/Si quantum-well has been designed for operation at $\lambda_0 = 1.55\ \mu m$. This single quantum-well modulator has a lower $V_\pi L_\pi$ than the 3 quantum-well modulator recently designed and optimized by Maine *et al.* for operation at $\lambda_0 = 1.31\ \mu m$, for which the $V_\pi L_\pi$ product was $1.8\ V \cdot cm$. This single quantum-well modulator contains a $Si_{0.8}Ge_{0.2}$ quantum-well with Non-Intentionally Doped (NID) and P^+ highly doped layers on either side. With no field applied, holes from the P^+ layers are captured by and confined in the quantum-well and when a reverse bias is applied holes are released from the quantum well and drift to the P^+ contact layer. Variations of the hole distribution lead to changes in the free-carrier absorption and the refractive index of each layer and subsequently to phase modulation of guided TE modes. The $V_\pi L_\pi$ product of the single quantum-well modulator is estimated $1.09\ V \cdot cm$ for low voltage linear modulation and $1.208\ V \cdot cm$ for 0 to $1.6\ V$ digital modulation, whereas the 3 quantum-well modulator gives a $V_\pi L_\pi$ of $2.039\ V \cdot cm$ for 0 to $6\ V$ digital modulation for operation at $\lambda_0 = 1.55\ \mu m$. Also, the optical loss in the single quantum-well ($5.36\ dB/cm$ at $V = 0\ V$) is lower than that of the 3 quantum-well structure ($5.75\ dB/cm$ at $V = 0\ V$). This single quantum-well modulator should also offer higher frequency operation than the 3 quantum-well modulator.

1. INTRODUCTION

Metal interconnects have become the primary bottleneck for the improvement of microprocessor performance due to their RC delay and high power consumption.[1] Optical interconnects offer a promising way to alleviate this bottleneck.[1] Silicon-based materials are the best platform for the various components of on-chip optical interconnects. Due to their Complementary Metal-Oxide-Semiconductor (CMOS) compatibility, both the electronic circuit and photonic circuit can be grown monolithically on the same substrate, reducing the cost.[2] Moreover, stronger optical confinement can be obtained with Silicon On Insulator (SOI) waveguides due to the higher refractive index contrast between Si and SiO_2 as compared to those obtained with III-V based optical interconnects grown on Si substrates.[3] One of the pivotal components of future optical interconnects are optical modulators. Various techniques have been developed to obtain optical modulation from Si and Si-based materials. Recently electroabsorption modulators were reported that used the quantum confined stark effect [4] or used the Franz Keldysh effect.[5] Typically electroabsorption modulators suffer from chirp which can be reduced by using electrorefraction modulators as these modulators can be implemented in a Mach-Zehnder push-pull configuration. To date, the free-carrier depletion effect[6] has become the most commonly used approach to obtain the electrorefraction effect in Si-based materials. Multiple configurations have been developed by various groups using this free-carrier depletion effect. [7–10] However, the $V_\pi L_\pi$ product, which is commonly used as the figure of merit, is quite high in these devices. Recently SiGe/Si modulation-doped[11] quantum-well optical modulators based on the free-carrier depletion effect were studied for operation at $\lambda_0 = 1.31\ \mu m$[12–15] by Marris *et al.* which are very promising due to their low drive voltage, small length and low free-carrier absorption loss. They also designed these quantum-well modulators for operation at $\lambda_0 = 1.55\ \mu m$[16] but the design was not optimized. They have also fabricated this structure and have conducted some experiments on it [16] which shows that the effective index variation depends on both the refractive index change of the layers and the thermal heating of the device.

In this paper, we designed a single quantum-well modulator giving a $V_\pi L_\pi$ of $1.09\ V \cdot cm$ for operation at $\lambda_0 = 1.55\ \mu m$. This structure has a much lower $V_\pi L_\pi$ than the most recent published structure designed and optimized by Maine *et al.* for operation at $\lambda_0 = 1.31\ \mu m$.[17] We have based our single quantum-well structure design on their 3 quantum-well structure.[18]

Photonics North 2010, edited by Henry P. Schriemer, Rafael N. Kleiman, Proc. of SPIE Vol. 7750,
77501N · © 2010 SPIE · CCC code: 0277-786X/10/$18 · doi: 10.1117/12.870014

Downloaded from SPIE Digital Library on 30 May 2011 to 137.82.117.28. Terms of Use: http://spiedl.org/terms

2. DESIGN OF THE SiGe/Si OPTICAL MODULATOR

Marris $et\ al.$ designed a 3 quantum-well modulator for operation at $\lambda_0 = 1.31\ \mu m$ using coupled electrical-optical simulations in Ref. [18] (in which they provided all of the physical parameters of their design as well as key operating values, which we will use for comparison). We re-analyzed the same structure for operation at $\lambda_0 = 1.31\ \mu m$. Our result (effective index variation at $V = 6\ V$) was consistent with their result. We then repeated the analysis of this structure for operation at $\lambda_0 = 1.55\ \mu m$, which gives a much lower $V_\pi L_\pi$. For this structure we found that the quantum-wells are being depleted sequentially, and one at a time, with the application of voltage which is also noted in Ref. [18]. Therefore, we designed a single quantum-well structure keeping the thickness and doping level constant for every layer. This structure leads us to a much lower $V_\pi L_\pi$ and higher frequency operation as compared to those obtained for the 3 quantum-well structure for operation at $\lambda_0 = 1.55\ \mu m$.

In this section, we will describe the general structure of these modulators followed by the coupled electrical-optical analysis used to design these modulators. We performed the electrical analysis in two different modes: DC analysis and transient analysis. We performed the DC analysis in order to investigate the electrical and optical behaviors of the device with the application of various reverse bias voltages. For this analysis we varied the applied reverse voltage from $0\ V$ to $10\ V$ ($10\ V$ is smaller than the simulated voltage breakdown). Then we performed the transient analysis in order to investigate the frequency response of the device. For this analysis, at first a reverse bias voltage step from 0 to $x\ V$ (where $x = 6$ for the 3 quantum-well modulator and 1.6 for the single quantum-well modulator) with a rise time of $1\ fs$ is applied to the device and the electrical and optical behaviors of the device are observed at several times ranging from 0 to $100\ ps$. Then, a reverse bias voltage step from x to $0\ V$ with a fall time of $1\ fs$ is applied to the device and the electrical and optical behaviors of the device are observed at several times for the next $100\ ps$. The results obtained using the DC analysis for the 3 quantum-well modulator and the single quantum-well modulator are described in section 3. The transient response for the 3 quantum-well modulator and the single quantum-well modulator are described in section 4.

2.1 Device Structure

The modulator consists of a P-Intrinsic-N (PIN) diode; the active region consists of 'k' periodic stacks of layers (where $k = 3$ for the 3 quantum-well modulator and 1 for the single quantum-well modulator). Each period consists of a $10\ nm$ $Si_{0.8}Ge_{0.2}$ quantum-well surrounded by $10\ nm$ Si-NID (Non-Intentionally Doped-$10^{16}\ cm^{-3}$) layers and $5\ nm$ P^+ highly doped ($2 \times 10^{18}\ cm^{-3}$) layers ($P^+$-$\delta$-doped layers). The PIN diode (thickness t) is grown on a $30\ nm$ Si-NID layer at the bottom of the PIN diode.[14] This structure is simulated using a $700\ nm$ SiO_2 layer, which is thick enough to prevent the light leaking towards the Si substrate.[19] For the lateral confinement of light, a rib structure is defined using the partial etching of the upper layers. The dimensions of the rib structure are defined such that this modulator can be integrated with a single mode SOI rib waveguide.[19] The mole fraction of Ge is chosen to be 0.2 to keep the bandgap of SiGe higher than the energy of the incident light to avoid band-to-band absorption and to maintain the total thickness below the critical thickness.[14]

2.2 Electrical and Optical Analysis

With no field applied, holes from the P^+ layers are captured by and confined in the quantum-wells and when a reverse bias is applied holes are released from the quantum wells and drift to the $30\ nm$ P^+ contact layer. Variation of the hole distribution leads to a free-carrier absorption change and a refractive index change in each layer and, subsequently, the phase modulation of the guided optical wave. We calculated the hole distribution in the various layers of the structure using Silvaco ATLAS^{TM}.[20] The solution of Poisson-Fermi-Schroedinger equations is needed for the calculation of the hole density in the quantum-wells of the SiGe/Si modulator.[21] However, it was shown by Marris $et\ al.$ (in Ref. [18]) that, if the quantum-well is equal to or thicker than $10\ nm$, the hole density profile in the structure at $V = 0\ V$ obtained by solving the Poisson-Fermi-Schroedinger equations is similar to that obtained by solving the Poisson-Fermi equations. That is why we used the Poisson-Fermi solver in Silvaco ATLAS^{TM} for the calculation of the hole density distribution at various applied voltages. The carrier transport in bulk material and at heterojunctions is calculated, respectively, using the drift-diffusion expressions and thermionic emission expressions.[22,23] The models used by Marris $et\ al.$ are the concentration dependent SRH (Shockley-Read-Hall) recombination model, the concentration dependent mobility model, the Auger model, and the Fermi-Dirac statistics model.[18] We used these models as well as two additional models: the field dependent mobility model and the band gap narrowing model. These additional models do not affect the DC analysis, but the field dependent mobility model affects the transient analysis as described in section 4. Experimental results show that higher reverse bias voltages

Downloaded from SPIE Digital Library on 30 May 2011 to 137.82.117.28. Terms of Use: http://spiedl.org/terms

lead to higher reverse leakage currents, and, therefore, higher leakage power that might create a self heating of the device which, in turn, affects the effective index variation.[16] This thermo-optical index variation becomes more significant at higher reverse bias voltages. However, as well as Marris $et\ al.$, we ignored these effects in our calculations. The material parameters used for this simulation are the default parameters for Si and $Si_{0.8}Ge_{0.2}$ used in Silvaco ATLAS^{TM}. We have tuned the bandgaps of these materials to be $E_{G-Si} = 1.12\ eV$ and $E_{G-Si_{0.8}Ge_{0.2}} = 0.972\ eV$ as defined in Ref. [14] and also the electron affinities to be $\chi_{Si} = 4.05\ eV$ and $\chi_{Si_{0.8}Ge_{0.2}} = 4.04\ eV$.[24]

The hole concentration obtained using the electrical simulation in Silvaco ATLAS^{TM} is averaged in each layer at each applied voltage.[12] As the layers are very thin, this approximation gives a refractive index profile similar to the refractive index profile obtained using the actual hole concentration profile. The absorption coefficient variation and refractive index variation in the doped Si layers with respect to undoped Si at $\lambda_0 = 1.55\ \mu m$, is calculated from the hole distribution using the following formulae[10]

$$\Delta\alpha = 8.5 \times 10^{-18}\Delta N + 6.0 \times 10^{-18}\Delta P \tag{1}$$

$$\Delta n = -8.8 \times 10^{-22}\Delta N - 8.5 \times 10^{-18}\Delta P^{0.8} \tag{2}$$

where ΔN and ΔP are, respectively, the electron and the hole concentration variations (cm^{-3}) with respect to the intrinsic carrier concentration of every layer.

To calculate the absorption coefficient change and the refractive index change in $Si_{0.8}Ge_{0.2}$ we used equation 1 and 2 due to the unavailability of separate equations for free carrier absorption for $Si_{0.8}Ge_{0.2}$.[25] The intrinsic hole concentration of Si and $Si_{0.8}Ge_{0.2}$ are, respectively, taken as $0.668 \times 10^{10}\ cm^{-3}$ and $10 \times 10^{10}\ cm^{-3}$, as defined in Silvaco ATLAS^{TM} at $T = 300^{o}K$. The refractive index of undoped Si and $Si_{0.8}Ge_{0.2}$ are taken as 3.475 and 3.505, respectively, for $\lambda_0 = 1.55\ \mu m$. The absorption coefficient for undoped Si and $Si_{0.8}Ge_{0.2}$ is considered to be negligible at $\lambda_0 = 1.55\ \mu m$. In our calculations, we considered only the hole concentration change in the various layers, as the electron concentration is negligible with respect to the hole concentration except in the N^+ layer, where the electron concentration is relatively high. For this N^+ layer, the refractive index and the absorption coefficient at $V = 0\ V$ is calculated from both ΔN and ΔP (ΔN is taken to be the doping density of this layer).

The free carrier absorption and the refractive index of each layer are used as the input to a mode solver,[26] which provides the effective index as well as the optical loss for TE polarized light at various voltages using the 2D semi-vectorial finite-difference approach.

3. DC ANALYSIS IN SiGe/Si MODULATORS

3.1 3 Quantum-Well SiGe/Si Modulator

A schematic diagram of the 3 quantum-well SiGe/Si modulator is shown in Fig. 1.

For the DC analysis, we applied reverse bias voltages ranging from $0\ V$ to $10\ V$ to this modulator. The hole distribution in the structure was calculated using Silvaco ATLAS^{TM} at each applied reverse bias voltage. The hole concentrations for the 3 quantum-well structure at several specific voltages are shown in Fig. 2. The absorption coefficient variation and refractive index variation in every layer is calculated from the hole distribution using equations 1 and 2, respectively.

Fig. 3(a) shows that the refractive index changes in the quantum-wells are much higher at $\lambda_0 = 1.55\ \mu m$ than at $\lambda_0 = 1.31\ \mu m$, which implies a higher effective index variation at $\lambda_0 = 1.55\ \mu m$. Fig. 3(a) shows that the refractive index change saturates with a saturation value of 1.6×10^{-3}, 1.95×10^{-3}, and 2.1×10^{-3} at $2.1\ V$, $4.3\ V$, and $7.5\ V$, respectively, in quantum-wells 1, 2, and 3 which indicates the depletion of the quantum wells. Also, Fig. 3(a) shows that the onset of the change in refractive index in each of the quantum-wells occurs near the saturation value of the preceding quantum-well. After the depletion of all 3 quantum-wells, the NID layer on the P^+ side starts depleting as well. The refractive index change in the NID layer is shown in Fig. 3(b).

The effective index variation curve for the 3 quantum-well structure is shown in Fig. 4(a). When the bias is lower than $7.5\ V$ the effective index variation in the modulator is mainly caused by the refractive index change in the quantum-wells. Above $7.5\ V$, the refractive index changes in all of the quantum-wells become constant but the contribution from the NID

Downloaded from SPIE Digital Library on 30 May 2011 to 137.82.117.28. Terms of Use: http://spiedl.org/terms

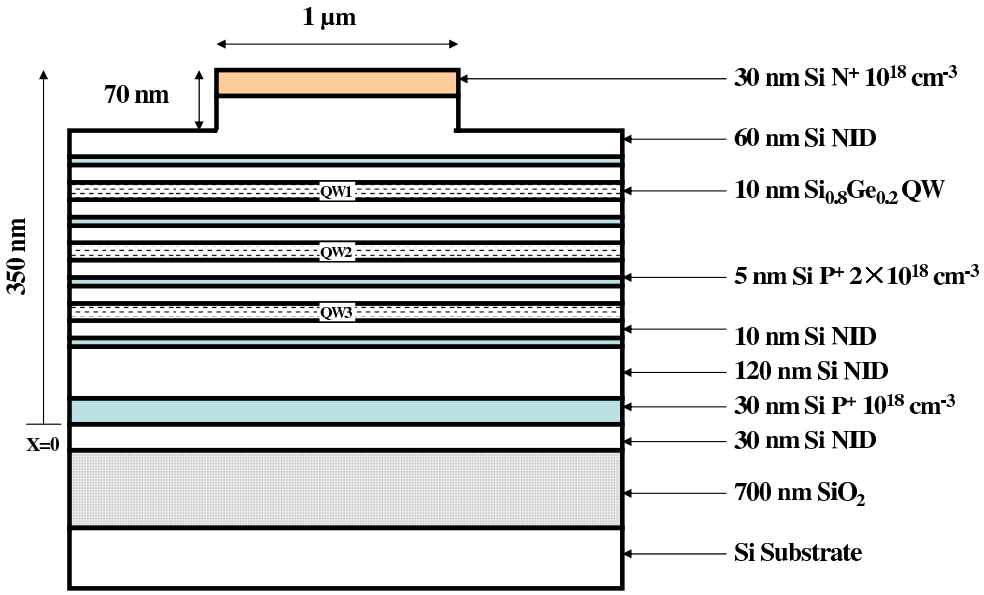

Figure 1. Schematic view of the 3 quantum-well SiGe/Si optical modulator.

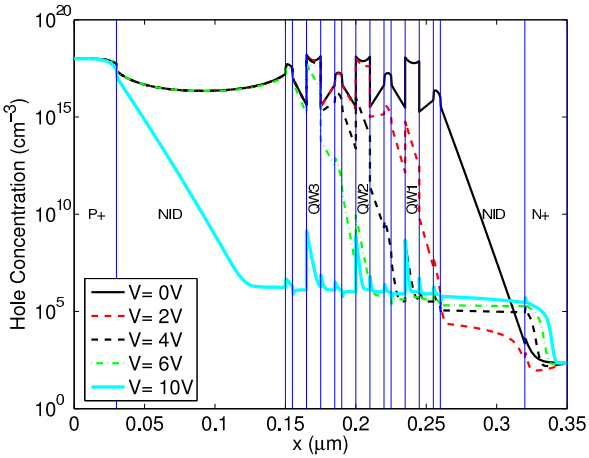

Figure 2. Hole distributions in various layers at various reverse bias voltages. With the increase in the reverse bias, holes deplete from the quantum-wells. Holes start to deplete from the NID layer on the P^+ side after all the quantum-wells are fully depleted $i.e.$, above $7.5\ V$ the NID layer starts to deplete.

layer on the P^+ side to the effective index variation becomes significant. In other words, after the depletion of all of the quantum-wells, the quantum-well modulator turns into a NID-layer modulator.

The two most important performance parameters obtained for this modulator are the effective index variation and optical loss which are found to be around 2.28×10^{-4} and 3.13 dB$/cm$ at $V = 6\ V$ for the wavelength of $\lambda_0 = 1.55\ \mu m$, as shown in Fig. 4(a) and Fig. 4(b), respectively. To evaluate the modulation efficiency of the phase modulator, a figure of merit is the $V_\pi L_\pi$ product, where V_π and L_π are, respectively, the applied voltage and the length required to obtain a π phase shift of the guided wave. An efficient modulator should posses a low $V_\pi L_\pi$ (for low drive voltage and/or small size) with low absorption losses. L_π can be calculated from the formula $L_\pi = \lambda_0/2\Delta n_{\text{eff}}$.[10] The effective index variation of 2.28×10^{-4} at $V = 6\ V$ leads to a $V_\pi L_\pi$ of $2.039\ V \cdot cm$ for the 3 quantum-well structure for $\lambda_0 = 1.55\ \mu m$, which is much lower than the $V_\pi L_\pi$ of $2.37\ V \cdot cm$ obtained for $\lambda_0 = 1.31\ \mu m$, predicted by our analysis, at $V = 6\ V$. The optical loss is slightly higher at $\lambda_0 = 1.55\ \mu m$, as compared to that at $\lambda_0 = 1.31\ \mu m$, which is consistent with the experimental results.[6]

Downloaded from SPIE Digital Library on 30 May 2011 to 137.82.117.28. Terms of Use: http://spiedl.org/terms

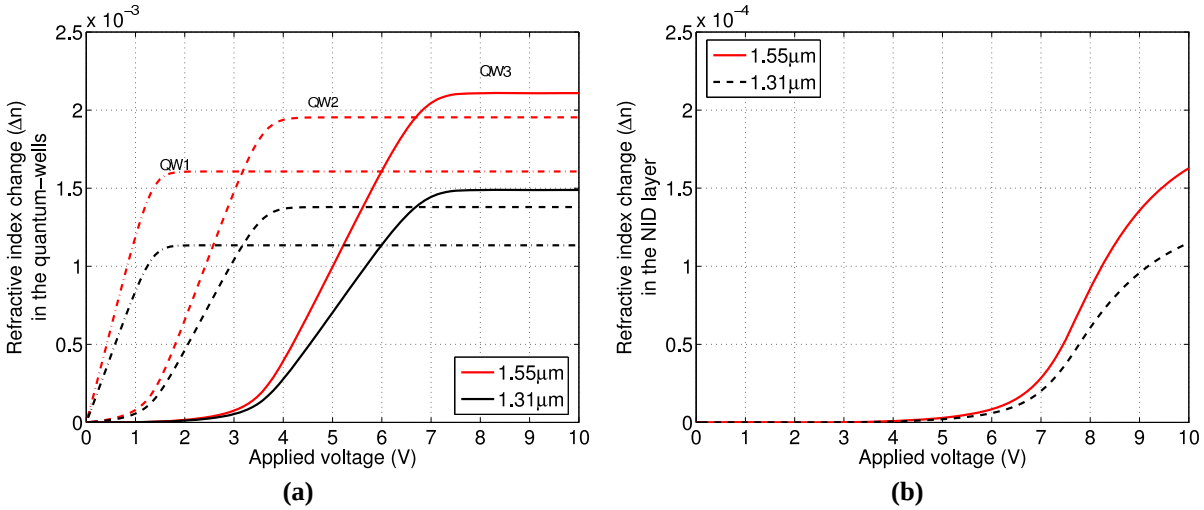

Figure 3. Refractive index changes ($\Delta n_v = n_v - n_0$) at $\lambda_0 = 1.55\ \mu m$ and $\lambda_0 = 1.31\ \mu m$ (a) in the quantum-wells, with a dash-dot line, a dotted line, and a solid line for quantum- well 1, 2, and 3, respectively (b) in the NID layer on the P^+ side.

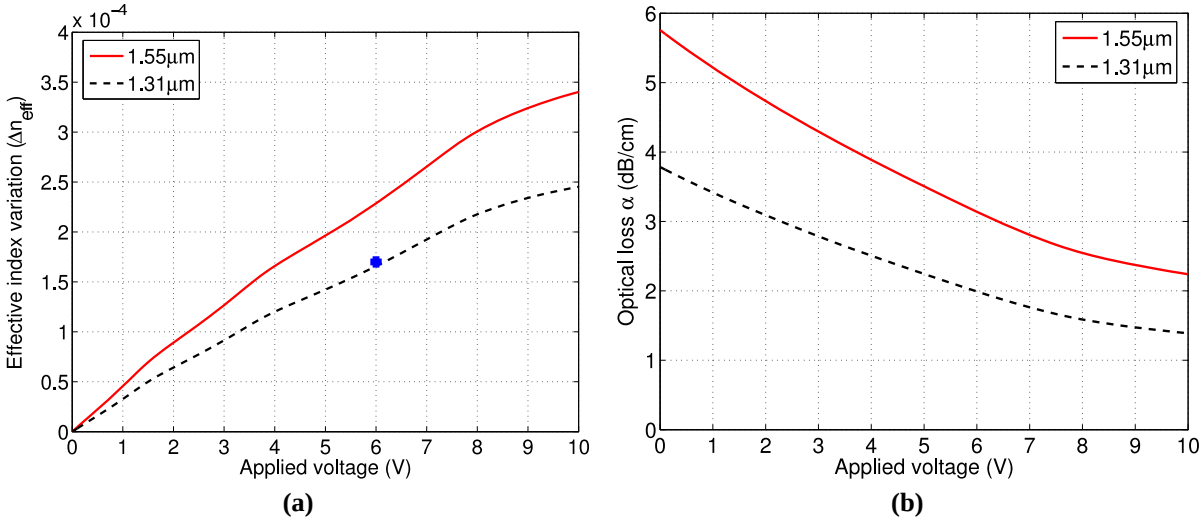

Figure 4. (a) Effective index variation ($\Delta n_{\text{eff-v}} = n_{\text{eff-v}} - n_{\text{eff-0}}$) of the 3 quantum-well modulator; the blue point shows the effective index variation at $6\ V$ obtained by Marris $et\ al.$ in Ref.[18] (b) optical loss at various voltages.

3.2 Single Quantum-Well SiGe/Si Modulator

A schematic diagram of the single quantum-well SiGe/Si modulator is shown in Fig. 5.

In the 3 quantum-well structure, when the voltage is lower than $V = 1.5\ V$, the effective index variation Δn_{eff} is mainly caused by the refractive index change in the first quantum-well. The onset of the change in the refractive index in the second quantum-well occurs after the refractive index change in the first quantum-well approaches its saturation value. This implies that only one quantum-well is needed to obtain the same effective index variation as that obtained in the 3 quantum-well structure for voltages below about $V = 1.5\ V$. Therefore, we designed a single quantum-well modulator keeping the thicknesses and doping levels constant for all of the layers ($i.e.$, 2 QW layer stacks were removed).

The refractive index change in the single quantum-well saturates at about $2\ V$ as shown in Fig. 6. The single quantum-well structure changes from a quantum-well modulator into a NID-layer modulator at this voltage.

The effective index variation curves and their slopes are shown in Fig. 7. Fig. 7(a) shows that below $2\ V$ the effective index variation in the single quantum-well structure is slightly higher than that in the 3 quantum-well structure. Above $2\ V$,

Downloaded from SPIE Digital Library on 30 May 2011 to 137.82.117.28. Terms of Use: http://spiedl.org/terms

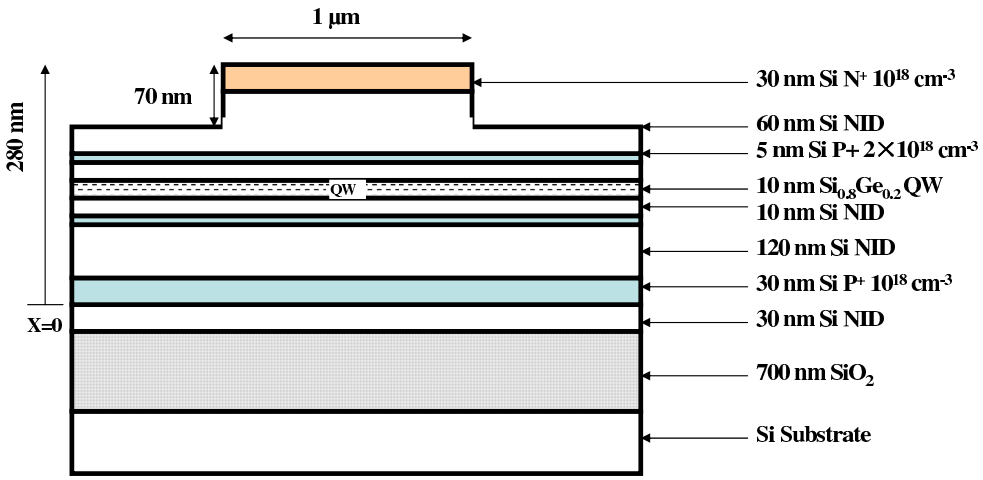

Figure 5. Schematic view of the SiGe/Si optical modulator.

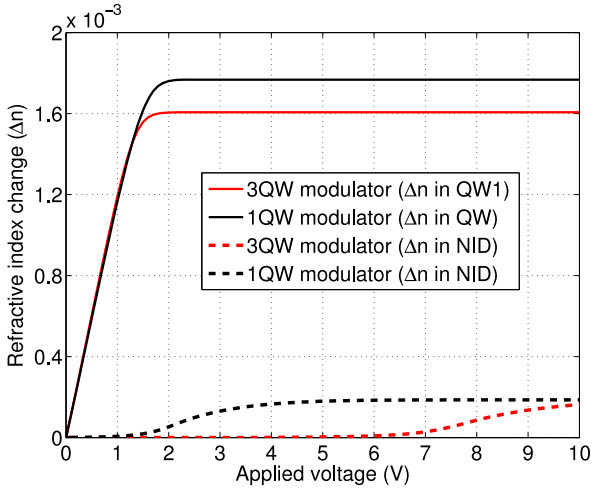

Figure 6. Comparison of the refractive index change in the single quantum-well structure and in the first quantum-well of the 3 quantum-well structure at $\lambda_0 = 1.55\ \mu m$. The refractive index change in the NID layers on the P^+ side are shown for both the single quantum-well and the 3 quantum-well modulator.

and considering only the refractive index changes in the quantum-wells, the effective index variation in the single quantum-well structure becomes smaller than that in the 3 quantum-well structure as shown by the dotted line in Fig. 7(a). However, due to the onset of the refractive index change in the NID layer on the P^+ side, the single quantum-well structure shows significantly higher effective index variation than the 3 quantum-well structure does until the cross-over point at about $6.5\ V$. Above $6.5\ V$, the 3 quantum-well modulator turns into a NID-layer modulator and the effective index variation in the 3 quantum-well structure becomes greater than that in the single quantum-well structure due to the combined effects of the refractive index changes in the quantum-wells and the NID layer. The optical loss in the single quantum-well structure is lower than that of the 3 quantum-well structure due to the removal of the two quantum-wells and the other doped layers. The optical losses for both of the structures are shown in Fig. 8.

The highest slope of the effective index variation ($0.71 \times 10^{-4}\ V^{-1}$) for the single quantum-well modulator occurs at about $1.6\ V$ as shown in Fig. 7(b). At this voltage the effective index variation is 1.02×10^{-4} with respect to $0\ V$. If we desire a V_π of $1.6\ V$ for digital signal modulation, the $V_\pi L_\pi$ of this modulator will be $1.208\ V \cdot cm$ which is much lower as compared to the $V_\pi L_\pi$ of the 3 quantum-well structure previously defined. For low voltage modulation, we can apply a voltage between $1.4\ V$ and $1.8\ V$ ($i.e.$, $\pm 0.2\ V$ from $1.6\ V$). Hence, if we desire such a V_π of $0.4\ V$ for low voltage modulation, the $V_\pi L_\pi$ of this modulator will be $1.09\ V \cdot cm$, which is also lower than the $V_\pi L_\pi$ of the 3 quantum-well modulator. This device can be further improved. Specifically, the location of the mode profile and the quantum-wells have

Downloaded from SPIE Digital Library on 30 May 2011 to 137.82.117.28. Terms of Use: http://spiedl.org/terms

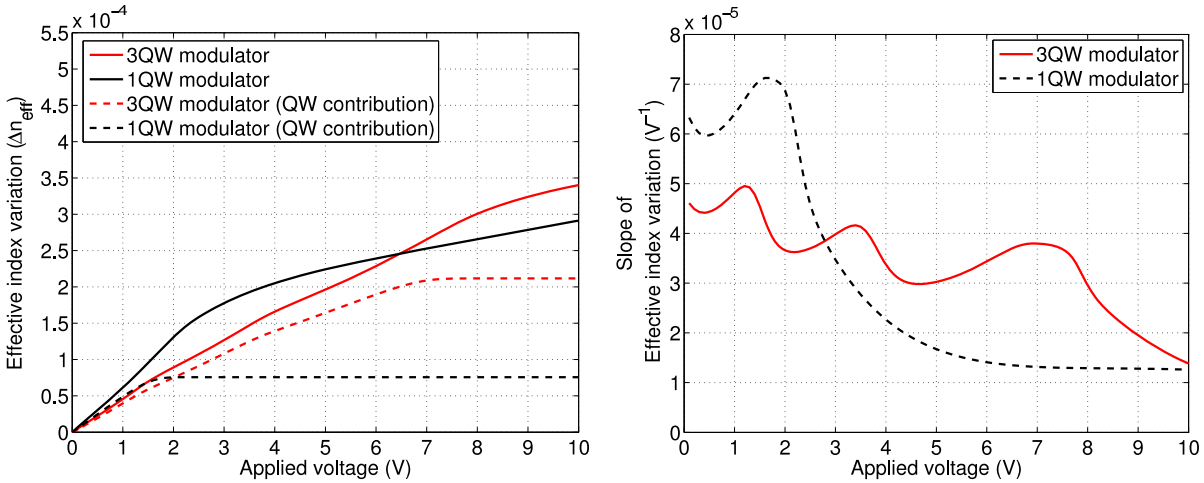

Figure 7. Comparison of the (a) Effective index variation (b) Slope of the effective index variation for single quantum-well and 3 quantum-well structure.

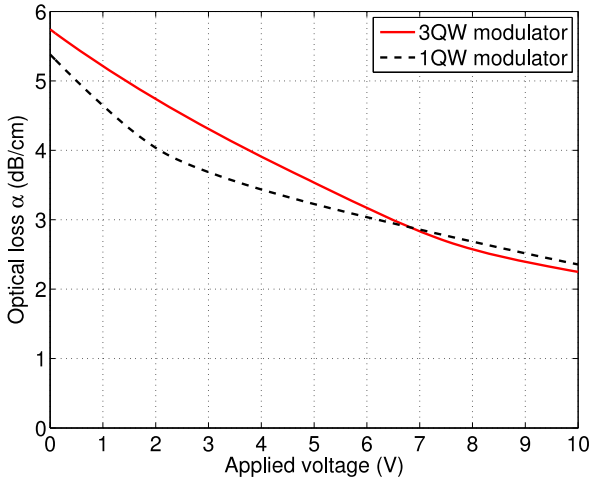

Figure 8. Comparison of the optical loss in the single quantum-well modulator and the 3 quantum-well modulator.

not been optimized. If we can improve the confinement factor, it can provide further improvement.

4. TRANSIENT ANALYSIS

Transient analysis is performed to evaluate the response time of the 3 quantum-well modulator and the single quantum-well modulator using thermionic emission, tunneling, and field dependent mobility model. Marris $et\ al.$ did not use the field dependent mobility model while doing the transient simulations.[18] But we found that, in case of transient analysis, the field dependent mobility significantly affects the transient response. The drift velocity of the carriers is the product of the mobility and the electric field in the direction of the current flow. The carrier velocity will increase with the increase of the electric field but at high electric fields, it will begin to saturate due to the reduction of the effective mobility. Hence, without using the field dependent mobility model, the response will be much faster than when using this model and the modulation speed will be overestimated.

For the 3 quantum-well modulator, at first, a reverse bias voltage step from 0 to $6\ V$, with a rise time of $1\ fs$, is applied to the device. The hole density distributions in the case of 3 quantum-well modulator obtained at several specific times, are plotted in Fig. 9(a). The holes are initially confined in the three quantum-wells at $t = 0$. As time increases, initially the

Downloaded from SPIE Digital Library on 30 May 2011 to 137.82.117.28. Terms of Use: http://spiedl.org/terms

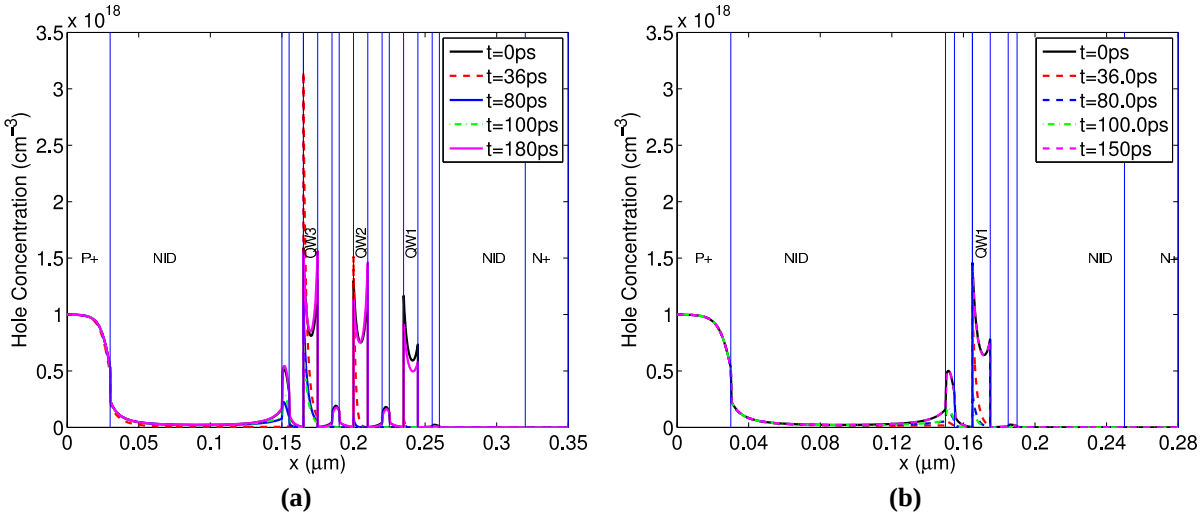

Figure 9. Hole density distribution with time in the (a) 3 quantum-well modulator (b) single quantum-well modulator.

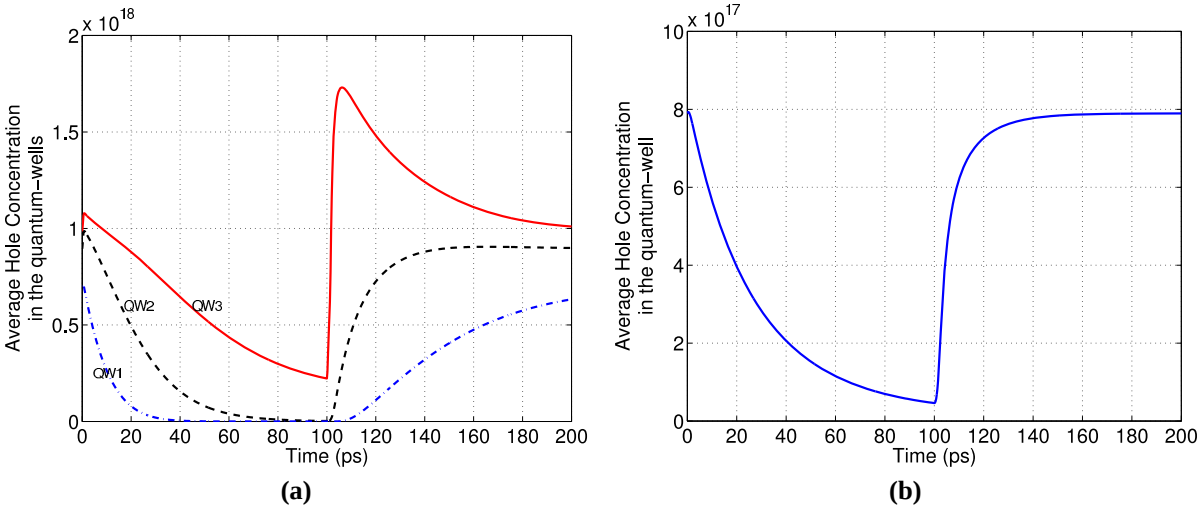

Figure 10. Hole density distribution with time (a) in the 3 quantum-well modulator for (b) in the single quantum-well modulator.

holes do not escape from the quantum-wells, they simply distribute themselves along the left side of each quantum-well. By $t = 36\ ps$ and $t = 80\ ps$ the 1st and the 2nd quantum-wells are depleted, respectively. By $t = 100\ ps$, only a few holes are left in the 3rd quantum-well. Fig. 10(a) shows that the quantum-wells are depleting sequentially in time as described in Ref. [18]. After $100\ ps$, the applied voltage returns to zero with a fall time $1\ fs$. The hole density distributions obtained at several specific times, during which the holes are returning to the quantum-wells, are plotted in Fig. 9(a). Fig. 10(a) shows that at $t = 150\ ps$, the average hole distribution becomes constant in the 2nd quantum-well and at $t = 180\ ps$, the hole density distribution in the 1st and in the 3rd quantum-well are approaching the constant value.

In the case of the single quantum-well modulator, at first, a reverse bias voltage step from 0 to $1.6\ V$, with a rise time of $1\ fs$, is applied to the device. The hole density distributions obtained at several specific times, are plotted in Fig. 9(b). The holes are initially confined in the quantum-well at $t = 0$. Most of the holes have been removed from the quantum-well by $t = 36\ ps$. By $t = 100\ ps$, only a few holes are left in the quantum-well as shown in Fig. 10(b). Hence, we can say that the hole depletion process is much faster in the case of the single quantum-well modulator than in the case of the 3 quantum-well modulator. After $100\ ps$, the applied voltage returns to zero with a fall time $1\ fs$. Fig. 10(b) shows that at $t = 140\ ps$, the average hole distribution becomes constant in the quantum-well.

The effective index variation curves for the 3 quantum-well modulator and the single quantum-well modulator are

Downloaded from SPIE Digital Library on 30 May 2011 to 137.82.117.28. Terms of Use: http://spiedl.org/terms

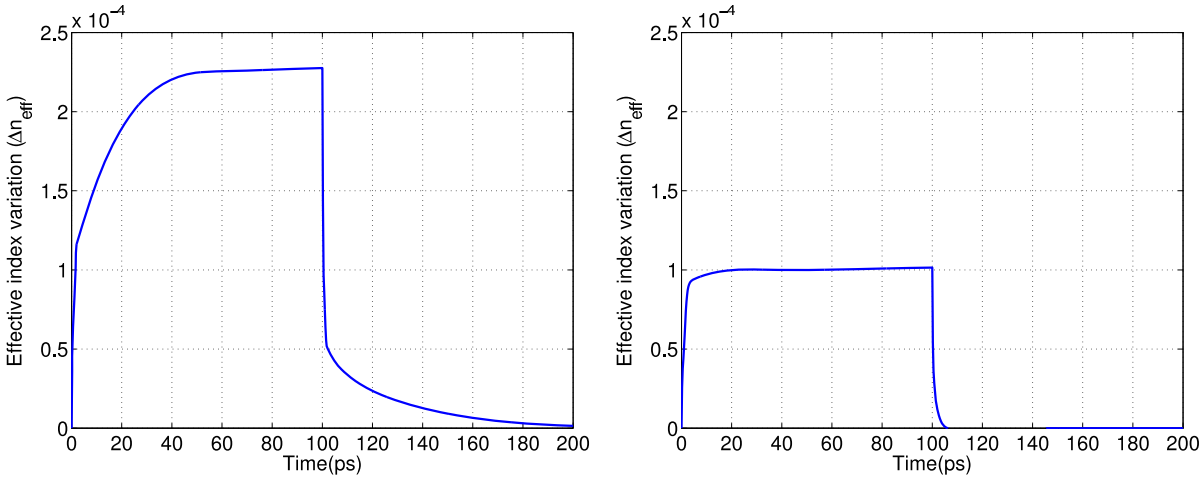

Figure 11. Effective index variation with time in (a) the 3 quantum-well modulator for 0 to 6 V variation and (b) in the single quantum-well modulator for 0 to 1.6 V variation.

shown in Fig. 11(a) and Fig. 11(b), respectively. From these figures we can conclude that transient response of the electrorefractive effect in the single quantum-well modulator will be faster than that in the 3 quantum-well modulator.

5. CONCLUSION

Using our DC analysis, we showed that the 3 quantum-well modulator gives a lower $V_\pi L_\pi$ for the wavelength of $\lambda_0 = 1.55$ μm as compared to the $V_\pi L_\pi$ obtained for $\lambda_0 = 1.31$ μm. We also verified that the quantum-wells in the 3 quantum-well structure deplete sequentially and one at a time with the application of voltage and, also, after the depletion of all of the quantum-wells, the quantum-well modulator turns into a NID-layer modulator. Then, we designed a single quantum-well modulator which gives a lower $V_\pi L_\pi$ as compared to the $V_\pi L_\pi$ of the 3 quantum-well modulator. Also, this single quantum-well modulator gives very high slope of the effective index variation before it turns into a NID-layer modulator. Finally, using our transient analysis, we showed that a faster step response can be obtained with the single quantum-well modulator than with the 3 quantum-well modulator.

REFERENCES

[1] Chen, G., Chen, H., Haurylau, M., Nelson, N. A., Albonesi, D. H., Fauchet, P. M., and Friedman, E. G., "Predictions of CMOS compatible on-chip optical interconnect," *Integration, the VLSI Journal* **40**, 434–446 (July 2007).

[2] Jalali, B., Yegnanarayanan, S., Yoon, T., Yoshimoto, T., Rendina, I., and Coppinger, F., "Advances in silicon-on-insulator optoelectronics," *Selected Topics in Quantum Electronics, IEEE Journal of* **4**(6), 938–947 (1998).

[3] Yang, V. K., Groenert, M. E., Taraschi, G., Leitz, C. W., Pitera, A. J., Currie, M. T., Cheng, Z., and Fitzgerald, E. A., "Monolithic integration of III-V optical interconnects on si using SiGe virtual substrates," *Journal of Materials Science: Materials in Electronics* **13**, 377–380 (July 2002).

[4] Kuo, Y., Lee, Y. K., Ge, Y., Ren, S., Roth, J. E., Kamins, T. I., Miller, D. A. B., and Harris, J. S., "Strong quantum-confined stark effect in germanium quantum-well structures on silicon," *Nature* **437**, 1334–1336 (Oct. 2005).

[5] Liu, J., Beals, M., Pomerene, A., Bernardis, S., Sun, R., Cheng, J., Kimerling, L. C., and Michel, J., "Waveguide-integrated, ultralow-energy GeSi electro-absorption modulators," *Nat Photon* **2**, 433–437 (July 2008).

[6] Soref, R. and Bennett, B., "Electrooptical effects in silicon," *Quantum Electronics, IEEE Journal of* **23**(1), 123–129 (1987).

[7] Liao, L., Samara-Rubio, D., Morse, M., Liu, A., Hodge, D., Rubin, D., Keil, U., and Franck, T., "High speed silicon Mach-Zehnder modulator," *Optics Express* **13**, 3129–3135 (Apr. 2005).

[8] Liu, A., Liao, L., Rubin, D., Nguyen, H., Ciftcioglu, B., Chetrit, Y., Izhaky, N., and Paniccia, M., "High-speed optical modulation based on carrier depletion in a silicon waveguide," *Optics Express* **15**(2), 660–668 (2007).

Downloaded from SPIE Digital Library on 30 May 2011 to 137.82.117.28. Terms of Use: http://spiedl.org/terms

[9] Marris-Morini, D., Vivien, L., Fdli, J. M., Cassan, E., Lyan, P., and Laval, S., "Low loss and high speed silicon optical modulator based on a lateral carrier depletion structure," *Optics Express* **16**(1), 334–339 (2008).

[10] Marris-Morini, D., Roux, X. L., Pascal, D., Vivien, L., Cassan, E., Fédéli, J. M., Damlencourt, J. F., Bouville, D., Palomo, J., and Laval, S., "High speed all-silicon optical modulator," *Journal of Luminescence* **121**, 387–390 (Dec. 2006).

[11] Daembkes, H., Herzog, H., Jorke, H., Kibbel, H., and Kaspar, E., "The n-channel SiGe/Si modulation-doped field-effect transistor," *IEEE Transactions on Electronic Devices* **33**, 633–638 (May 1986).

[12] Cordat, A., Lardenois, S., Thanh, V. L., and Koster, A., "SiGe/Si multiquantum well structure for light modulation," *Materials Science and Engineering B* **89**, 66–69 (Feb. 2002).

[13] Marris, D., Cordat, A., Pascal, D., Koster, A., Cassan, E., Vivien, L., and Laval, S., "Design of a SiGe-Si quantum-well optical modulator," *Selected Topics in Quantum Electronics, IEEE Journal of* **9**(3), 747–754 (2003).

[14] Marris, D., Cassan, E., Vivien, L., Pascal, D., Koster, A., and Laval, S., "Design of a modulation-doped SiGe/Si optical modulator integrated in a submicrometer silicon-on-insulator waveguide," *Optical Engineering* **44**(8), 084001–6 (2005).

[15] Maine, S., Marris-Morini, D., Vivien, L., Pascal, D., Cassan, É., and Laval, S., "Design optimization of SiGe/Si: modulation-doped multiple quantum well modulator for high-speed operation," **6183**, 10 (Apr. 2006).

[16] Lupu, A., Marris, D., Pascal, D., Cercus, J., Cordat, A., Thanh, V. L., and Laval, S., "Experimental evidence for index modulation by carrier depletion in SiGe/Si multiple quantum well structures," *Applied Physics Letters* **85**(6), 887–889 (2004).

[17] Maine, S., Morini, D. M., Vivien, L., Cassan, E., and Laval, S., "Design optimization of a SiGe/Si Quantum-Well optical modulator," *Journal of Lightwave Technology* **26**, 678–684 (Mar. 2008).

[18] Marris, D., Cassan, E., and Vivien, L., "Response time analysis of SiGe/Si modulation-doped multiple-quantum-well structures for optical modulation," *Journal of Applied Physics* **96**, 6109–6112 (Dec. 2004).

[19] Lardenois, S., Pascal, D., Vivien, L., Cassan, E., Laval, S., Orobtchouk, R., Heitzmann, M., Bouzaida, N., and Mollard, L., "Low-loss submicrometer silicon-on-insulator rib waveguides and corner mirrors," *Optics Letters* **28**, 1150–1152 (July 2003).

[20] *http://www.silvaco.com/products/device_simulation/atlas.html*.

[21] Tan, I., Snider, G. L., Chang, L. D., and Hu, E. L. *Journal of Applied Physics* **68**(8), 4071 (1990).

[22] Grupen, M., Hess, K., and Song, G., "Simulation of transport over heterojunctions," in [*Proc. 4th International Conf. Simul. Semicon. Dev. Process*], **4**, 303–311.

[23] Horio, K. and Yanai, H., "Numerical modeling of heterojunctions including the thermionicemission mechanism at the heterojunction interface," *IEEE Transactions on Electron Devices* **37**(4), 1093–1098 (1990).

[24] *http://www.virginiasemi.com/pdf/generalpropertiesSi62002.pdf*.

[25] Vonsovici, A. and Vescan, L., "Modulation doped SiGe-Si MQW for low-voltage high-speed modulators at 1.3 m," *Selected Topics in Quantum Electronics, IEEE Journal of* **4**(6), 1011–1019 (1998).

[26] Fallahkhair, A., Li, K. S., and Murphy, T. E., "Vector finite difference modesolver for anisotropic dielectric waveguides," *Journal of Lightwave Technology* **26**, 1423–1431 (June 2008).

Downloaded from SPIE Digital Library on 30 May 2011 to 137.82.117.28. Terms of Use: http://spiedl.org/terms